EFDA–JET–CP(10)08/01

F. Romanelli, M. Laxåback
and JET EFDA contributors

Overview of JET Results

Overview of JET Results

F. Romanelli, M. Laxåback[1]
and JET EFDA contributors*

JET-EFDA, Culham Science Centre, OX14 3DB, Abingdon, UK

[1]Association EURATOM-VR, EES, KTH, SE-10044 Stockholm, Sweden
** See annex of F. Romanelli et al, "Overview of JET Results",*
(23rd IAEA Fusion Energy Conference, Daejon, Republic of Korea (2010)).

Preprint of Paper to be submitted for publication in Proceedings of the
23rd IAEA Fusion Energy Conference, Daejon, Republic of Korea
(10th October 2010 - 16th October 2010)

ABSTRACT.
Since the last IAEA Conference JET has been in operation for one year with a programmatic focus on the qualification of ITER operating scenarios, the consolidation of ITER design choices and preparation for plasma operation with the ITER-like wall presently being installed. Good progress has been achieved, including stationary ELMy H-mode operation at 4.5MA. In matched NBI+ICRF heated H-mode plasmas with up to 100% of ICRF heating the confinement was found to be independent of the heating mix. The high confinement hybrid scenario has been extended to high triangularity, lower ρ^* and to pulse lengths comparable to the resistive time. The steady-state scenario has also been extended to lower ρ^* and ν^* and optimised to simultaneously achieve, in stationary conditions, ITER-like values of all other relevant normalised parameters. Dedicated physics studies have demonstrated reduced core ion stiffness in plasmas with high rotational, and low magnetic, shear, allowing gradients with normalised ion temperature gradient lengths up to 8 in the fastest rotating hybrid discharges. Effective sawtooth control by fast ions has been demonstrated with ^{3}He minoity ICRH, a scenario with negligible minority current drive. ELM control studies using external n = 1 and n = 2 perturbation fields have found a resonance effect in ELM frequency for specific q_{95} values. Complete ELM suppression has however not been observed, even with an edge Chirikov parameter larger than 1. Pellet ELM pacing has been demonstrated and the minimum pellet size needed to trigger an ELM has been estimated. In disruption studies with Massive Gas Injection up to 50% of the thermal energy could be radiated before, and 20% during, the thermal quench. Halo currents could be reduced by 60% and, using argon/deuterium and neon/deuterium gas mixtures, runaway electron generation could be avoided. Most objectives of the ITER-like ICRH antenna have been demonstrated; matching with closely packed straps, ELM resilience, Scattering Matrix Arc Detection and operation at high power density (6.2MW/m^2) and antenna strap voltages (42kV). Coupling measurements are in very good agreement with TOPICA modelling.

1. INTRODUCTION

Since the last IAEA Conference [1] JET has been in operation for one year with a maintained programmatic focus on the qualification of ITER operating scenarios [2], the consolidation of ITER design choices and the preparation for future plasma operation with the JET ITER-like Wall [3, 4]. Machine and sub-system reliability has been very good (with neutral beam power in excess of 22MW being achieved in several pulses) and has allowed strong progress in the JET Programme, including stationary Type I ELMy H-mode operation with plasma currents up to 4.5MA [5] and a dedicated Helium campaign to evaluate key aspects of plasma control and H-mode operation for the ITER non-activated phase. The latest experimental campaign ended in October 2009 and JET has since been in shutdown for the JET Enhancement Programme 2 (EP2) upgrades, chiefly the installation of the ITER-like Wall (ILW) and the upgrade to the Neutral Beam Injection (NBI) system [6]. The ILW project sees the replacement of all Carbon Fibre Composite (CFC) Plasma Facing Components (PFCs) with beryllium for the first wall (solid Be and 8μm Be-coated Inconel) and tungsten in the divertor (10-15μm and 20-25μm W-coated CFC tiles for the inner and outer divertor respectively [7,8], and bulk W for the horizontal tile for the outer strike point in high

performance scenarios [9, 10]). The Neutral Beam upgrade will bring the maximum power from 22MW to 34MW with the pulse length extended to 20s. Before the end of the campaign the new Enhanced Radial Field Amplifier [11] (together with a few new diagnostics) have been installed and fully commissioned [12], demonstrating its capability of controlling plasma vertical position with the largest Edge Localised Modes (ELMs) [13]. Installation tasks for the EP2 upgrades are scheduled to be completed by the end of 2010, with plasma operation restarting in 2011.

2. PROGRESS IN THE QUALIFICATION OF ITER OPERATING SCENARIOS

2.1 ELMY H-MODE

The dependence on the edge pedestal and ELM characteristics on the normalised ion gyroradius $\rho^* = \rho_i / a$ have been explored in joint JET and DIII-D experiments. Taking advantage of the difference in machine size a factor 4 variation in ρ^* was achieved, keeping other dimensionless parameters (ν^* and β_{pol}) at the top of the H-mode pedestal fixed [14,15]. The results rule out a strong dependence of the pedestal width on ρ^* which is predicted by some theoretical models [14].

Following earlier observations of a dependence of the fractional ELM losses on ρ^* in DIII-D [16], a specific attempt has been made to elucidate a similar dependence on JET. As shown in Fig.1, the JET DIII-D comparison seems to point out a size dependence of the fractional ELM losses, although JET data alone seems to have little or no dependence on ρ^*. The scaling of ELM sizes to ITER thus remains an open issue, pointing out the need on ITER for a robust and flexible ELM suppression/mitigation system.

Extrapolations from present day devices to the ITER $Q_{DT} = 10$ baseline scenario are based predominantly on ELMy H-modes heated by positive NBI with dominant ion-heating and significant toroidal momentum input. In contrast, plasma heating in ITER will be by α-particles, negative NBI, Ion Cyclotron Resonance Heating (ICRH) and Electron Cyclotron Resonance Heating (ECRH) with dominant electron heating and insignificant levels of momentum input. Exploiting the recent improvements in resilience of the JET ICRH systems (see Sec. 5) to ELMs the effect of heating mix and rotation on the confinement has been investigated in matched pairs of NBI-only and NBI + ICRF-heated low triangularity ($\delta = 0.25$) 2.5 MA / 2.7 T ($q_{95} \sim 3.6$) H-mode plasmas [17]. In increasing the fraction of ICRH power from 50% ($P_{tot} \sim 16$ MW, $P_{loss} / P_{L-H} \sim 2$) to 100% ($P_{tot} \sim 9$ MW, $P_{loss} / P_{L-H} \sim 1.2$) no significant differences were found compared to the matched NBI-only plasmas. The plasma confinement is found to be independent of the heating mix, Fig.2, density and temperature profiles in the core are similar and $T_i \approx T_e$ despite the different heat, particle and torque deposition profiles. The pedestal pressure is also independent of the heating mix and there is no obvious correlation between the ELM size / frequency and the heating mix. The toroidal rotation in the ICRH-dominated plasmas was approximately 10 times lower at the edge and 5 times lower in the core. The plasma density in these discharges was around 65% of the Greenwald density and Z_{eff} was typically 1.7 - 2.

2.2 HYBRID SCENARIO

The hybrid scenario is a promising route for ITER because it might allow the achievement of Q=10 at lower plasma current and for longer pulses than the baseline scenario. At the 2008 IAEA FEC

it was reported that confinement enhancement up to 40% above the IPB98(y,2) scaling [18] was transiently achieved. Using a current ramp-down technique prior to the main heating phase to tailor the target q-profile JET hybrid plasmas now routinely achieve confinement improvements over the standard H-mode. Since 2008 the hybrid scenario has been extended to high triangularity ($\delta \sim 0.4$) and lower ρ^* ($\rho^* \sim 3.5\times10^{-3}$) at 2.3T and up to 2MA [19]. Pulse lengths in excess of 6 s ($\sim\tau_R$) have been achieved at $f_{Greenwald} \sim 0.75$ and $\beta_N \sim 3$. Improved confinement has been obtained with H_{98} approaching 1.3 - 1.4 in plasmas where MHD and plasma-wall interactions were avoided. In these conditions low magnetic shear in presence of high rotation may also lead to reduced ion stiffness and contribute to the overall confinement (see Sec 3.1).

2.3 ADVANCED TOKAMAK / STEADY-STATE SCENARIO

The performance and stability of the advanced tokamak scenario with Internal Transport Barrier (ITB) has been extended to 1.8MA / 2.7T ($q_{95} \sim 4.7$), achieving dimensionless parameters approaching the ITER steady-state targets for high triangularity ($\delta \sim 0.4$) plasmas with global $\rho^* / \rho^*_{ITER} \sim 2$ and $\nu^* / \nu^*_{ITER} \sim 4$ [20], Fig. 4. In addition to around 22MW of NBI, up to 8MW of ICRH and typically 2.5MW of LHCD was applied to a $q_0 \sim 2$ target chosen to optimise the bootstrap current. Relatively weak ITBs are formed (typically correlated with the $q = 2$ surface rather than with negative shear) allowing to simultaneously achieve $\beta_N \geq 2.7$, $H_{98} \geq 1.2$, $T_e \sim T_i$, $f_{bootstrap} \sim 0.4$, $f_{Greenwald} \sim 0.65$ and a large thermal energy fraction, $f_{TH} \sim 0.8$, in stationary conditions ($\sim 10\ \tau_E$). Gas injection added to improve the ICRH and LHCD coupling lead to Type I ELMs about 40% smaller than natural ELMs and clean plasma conditions, $Z_{eff} \leq 2$. In all discharges there is however evidence that the q-profile is evolving, signifying a shortage of non-inductive current. TRANSP interpretive modelling indicates a bootstrap fraction in the range of 36 – 45% and NBI current drive of 20% of the plasma current. An additional 35% of non-inductive current drive would therefore be needed to make these scenarios fully steady-state. Predictive CRONOS [21] modelling indicates that it would be possible to maintain the q-profile needed to sustain the ITB, and hence maintain the performance, with the off-axis current drive that could be provided by the recently proposed ECRH / ECCD system for JET [22].

2.4 QUALIFICATION OF HELIUM OPERATION FOR THE ITER NON-ACTIVATED PHASE

During the initial non-activated phase, ITER must operate either hydrogen (H) or helium (^{4}He) plasmas to commission systems, evaluate ELM-mitigation techniques and develop operating scenarios for DT operation. The high L-H power threshold in hydrogen (around twice that in deuterium) appears to preclude hydrogen H-mode operation in ITER, leaving helium as the likely choice. A dedicated helium campaign with the NBI system fully converted to helium has been carried out at JET, using the technique of argon frosting for both divertor and NBI cryopumps to ensure helium pumping, in order to qualify plasma scenarios in helium.

The L-H power threshold of matched 1.7MA / 1.8T deuterium and helium discharges was found to be ~4MW at $n_e = 2.5 - 2.9\times10^{19}$ m^{-3}, irrespective of the helium concentration [23]. At lower density,

$n_e = 2.1\times10^{19}$ m^{-3}, the threshold was however higher in helium than deuterium. The threshold power for Type III to Type I ELMs was also similar for both gasses, approximately twice the L-H power threshold. Scaled to the ITER half-field baseline scenario (7.5 MA / 2.65 T, $f_{Greenwald} = 85\%$) using the Martin08 scaling [24] the L-H power threshold in helium should be 30 - 42 MW (or 20 – 65 MW for an appropriately chosen 95% confidence interval). The power threshold for Type I to Type III ELMs would correspondingly be 42 – 48MW (23 - 86MW). For a matched helium/deuterium pair of discharges, the pedestal width was found to be similar, 2.1±0.5 cm in helium and 2.5±0.5 cm in deuterium, but the pedestal pressure in helium was only 70% of that in deuterium. Correspondingly, the energy confinement in helium plasmas normalised to the IPB98(y,2) scaling law was found to be around 70% of the confinement in deuterium.

Heat load studies of the outer divertor target using a fast high resolution infrared camera revealed that while the radial ELM heat load profiles are similar for helium and deuterium plasmas, the inter-ELM and time averaged heat load profiles are broader with helium. The power arrival time / heat pulse durations for helium are also much longer, leading to lower peak heat loads [25].

Helium operation also allowed the flux consumption and heating requirements for current profile control during the current-rise, $q_{95} = 3$ flat-top and ramp-down in ITER helium plasmas to be assessed [26]. JET performed ITER scenario demonstration discharges in deuterium in 2008 [27] that contributed to the modification of the ITER coil design and have been used as a reference for the helium discharges. Good control of the internal inductance is achieved with both gasses during the current ramp-up using a full bore plasma shape with early X-point formation at 0.8MA, equivalent to forming a diverted plasma at 4.5 MA in ITER. Early heating is required to keep li below 0.85 when using the fastest current ramp rate available (0.36 MA/s), still maintaining an MHD stable plasma up to $q_{95} = 3$ with a transition to H-mode that in JET deuterium discharges occurs at 7 - 9MW and in helium at 8 - 11MW. During the current ramp-down the plasma inductance can be maintained within the ITER limits by remaining in H-mode. If heating is not available, simultaneous control of the internal inductance and avoidance of flux consumption can be achieved by combining an appropriate ramp-down rate with a strong reduction in plasma elongation to reduce the vertical instability growth rate. Apart from higher flux consumption for helium discharges during plasma initiation deuterium and helium discharges are very similar with respect to key requirements for ITER plasma control.

3. PLASMA TRANSPORT AND CORE STABILITY

3.1 MOMENTUM TRANSPORT AND INTRINSIC ROTATION

Plasma rotation is well known to have beneficial effects on MHD modes, such as resistive wall modes and neoclassical tearing modes, and sheared plasma rotation is an important factor in plasma turbulence stabilisation. The combination of sheared rotation and low magnetic shear for example appears to play a role in the improved core ion confinement observed in hybrid and advanced tokamak scenarios [28]. In light of the low external momentum input of the ITER 1MV NBI system, a robust understanding of momentum transport and intrinsic momentum sources and sinks is crucial.

The radial profiles of the inward momentum pinch and Prandtl number have been determined on JET using modulated NBI powers and torques and compared to linear gyro-kinetic code predictions using GKW [29] and GS2 [30], [31]. Quantitative agreement is found in the dependence of the pinch number, Rv_{pinch}/χ_ϕ (with R the torus major radius, v_{pinch} the pinch velocity and χ_ϕ the toroidal momentum diffusivity), and the diffusive Prandtl number, $P_r = \chi_\phi/\chi_i$, on the inverse density gradient length, $R/L_n = R|\nabla n|/n$. The dependence on other parameters is weak, and neither Rv_{pinch}/χ_ϕ nor P_r depends on collisionality. Rv_{pinch}/χ_ϕ is found to be between 3 and 5 around the plasma mid radius (r/a = 0.4 - 0.8), only increasing above 5 for $R/L_n > 3$. P_r, which does not depend significantly on any of the parameters scanned, is typically 1.5 - 2 at the plasma mid radius and increases with plasma minor radius.

In JET plasmas with normal toroidal magnetic field ripple, $\delta_{BT} = 0.08\%$, the intrinsic toroidal rotation in the absence of significant momentum injection by NBI is always small, $\omega_\phi < \pm 10$ krad/s, also in ICRH-dominated H-mode plasmas with β_N up to 1.3 [32]. This is in conflict with existing multi-machine scaling laws for the intrinsic rotation, which predict an Alfvén-Mach number an order of magnitude larger [33]. At the ITER ripple level, $\delta_{BT} = 0.5\%$, the JET intrinsic rotation is near zero. At higher toroidal field ripple the edge rotation is near-zero and the core is rotating in the counter-current direction, faster in plasmas with Type III than with Type I ELMs. A separate study has analysed the relative loss of toroidal momentum to plasma energy associated with ELMs, showing that the momentum losses are consistently larger than the energy losses, Fig. 5. The losses of momentum are observed to penetrate deeper into the plasma during large Type I ELMs than the losses of energy, r/a = 0.65 as compared to r/a = 0.8. As a result, the time averaged toroidal rotation at the top of the pedestal decreases with increasing ELM frequency.

3.2 SAWTOOTH STABILITY CONTROL

Effective sawtooth control has been demonstrated with ^{3}He minority ICRH with toroidally directed antenna spectra and the resonance tangential to the q = 1 surface [34]. Since the minority ion current drive for this scenario is expected to be negligible in JET (and in ITER) due to the electron drag current, this demonstrates the direct kinetic response of highly energetic ions on the internal kink mode. The effect is explained by fast ions with wide drift orbits intersecting the q = 1 surface predominantly on the high field side (good magnetic curvature) or low field side (bad magnetic curvature) due to asymmetric parallel velocity distributions [35]. Using 4 MW of ICRH the sawtooth period could be decreased (-90° antenna phasing) or increased (+90° antenna phasing) by more than a factor 2, Fig. 6. This direct effect of fast ions on the sawtooth stability is encouraging for ITER, where the ability of the ICRH system to control the magnetic shear by Ion Cyclotron Current Drive (ICCD) is expected to be weak [36].

4. FIRST WALL POWER AND PARTICLE LOADINGS

4.1 ELMS AND THEIR AMELIORATION

The understanding and mitigation of ELMs is one of the main issues for reliable ITER operation. ITER will require reliable ELM control over a wide range of operating conditions and it is therefore

essential to develop a suite of different ELM mitigation techniques. On JET, ELM control studies using Resonant Magnetic Perturbations (RMP) produced by the external Error Field Correction coils (EFCCs), rapid radial field changes ("vertical kicks"), gas injection and pellet pacing have progressed towards establishing the necessary conditions for mitigation, the impact on the plasma confinement and the effect on the divertor heat loads [37, 38, 39].

The application of EFCCs and kicks in high triangularity ($\delta = 0.43$) H-mode plasmas (2MA / 2.2 - 2.4T, $q_{95} = 3.6$ - 3.9, $P_{NBI} = 7$ - 12MW, $P_{ICRH} = 1$ - 2MW) with low natural ELM frequencies, f_{ELM} ~7 - 15 Hz, allows an increase in ELM frequency by a factor of 5 with kicks and 3.5 with EFCCs [37]. The increase in ELM frequency is associated with a decrease in the normalised energy loss per ELM, Fig. 7. Notably, all ELM control methods (EFCCs, kicks and gas) follow the same trend in $\Delta W_{ELM} / W_{PED}$ with f_{ELM} and the mitigated ELMs can be sustained also at low pedestal collisionality. Both EFCCs and kicks are associated with a density pump-out which reduces the core density by ~30%. This can be compensated for by gas puffing, but at a cost in confinement. Toroidal rotation braking (up to 50%) is observed extending over the whole plasma column with EFCCs, whereas with kicks a ~10% reduction in the edge rotation is found due to the increased losses of toroidal momentum at the higher ELM frequency, see Sec. 3.1.

On DIII-D, in-vessel RMP coils producing an $n = 3$ perturbation field allows Type I ELMs to be completely suppressed in narrow windows of the edge safety factor ($q_{95} = 3.5$ - 3.9 and $q_{95} \sim 7.2$) [40,41]. On JET, ELM control studies with $n = 1$ or $n = 2$ perturbation fields induced by the EFCCs have not yet shown complete ELM suppression, even in plasmas with edge vacuum Chirikov parameters greater than 1. In low triangularity plasmas ($\delta \sim 0.2$) a q_{95} scan at fixed toroidal field (1.84 T) and low pedestal collisionality ($\nu^* \sim 0.1$) however shows a resonance effect, where the ELM frequency increases a factor 4 - 5 at specific values of q_{95} with $n = 1$ fields applied. For non-resonant values of q_{95} the ELM frequency only increases a factor of about two with the $n = 1$ field applied [42,38], Fig. 8. The same effect is also found with an $n = 2$ field. This multiple resonance effect can be qualitatively predicted by a model in which the ELM width is determined by a localised relaxation to a profile which is stable to ideal external peeling modes.

Pellet pacing up to 10Hz has been demonstrated in 2.0MA / 2.3 T ($q_{95} = 3.8$) plasmas with 11 MW of NBI heating using the fuelling section (nominally 2.2×10^{21} D / pellet, 200m/s) of the High Frequency Pellet Injector (HFPI) for low field side injection. While the natural ELM frequency in these plasmas was also around 10 Hz, the ELMs were synchronised with the pellets - confirming the ELM pellet pacing technique on JET. The minimum pellet size (and thereby the minimum unavoidable fuelling) required to trigger ELMs has been estimated from the D_α signal from pellets with a large size scatter injected with the pacing section of the HFPI from the vertical high field side. The observations indicate that a pellet needs a mass greater than 1 - 1.6×10^{19} D to reliably trigger an ELM. According to modelling, pellets of this size should penetrate to at least half the pedestal width [43].

Fast high resolution infrared measurements on the outer divertor target have shown that the width of the ELM heat load profiles increases with relative ELM size, for natural as well as mitigated ELMs regardless of the mitigation method used. For small ELMs, the radial extent of the ELM heat

load profiles is 2.5 times broader than the inter-ELM value of ~4 mm. In all cases the ELM wetted area is larger than the inter-ELM area and the broadening increases with ELM size [44,45].

4.2 Disruption studies for ITER

The experimental disruption studies on JET have focussed on the understanding of asymmetric Vertical Displacement Event (VDE) disruptions and on disruption amelioration by Massive Gas Injection (MGI) as a means to reduce the impact of disruptions on the tokamak structure (electromagnetic forces from halo and eddy currents and localised heat loads from convection and runaway electrons) [46,47]. In addition, an extensive survey of all JET disruptions during the last decade has allowed the sequences of events and root causes of the dominant classes of disruptions to be identified [48].

During asymmetric VDE disruptions the plasma current and vertical current moment are n = 1 toroidally asymmetric, leading to sideways forces that in JET can be as high as 4 MN [49]. In most JET disruptions the plasma current asymmetry rotates in the counter-current direction at ~100Hz, although with large scatter. For ITER, the dynamic amplification of structural forces that would occur if the rotating modes resonated with the vessel at the 8 Hz fundamental mechanical vessel frequency is a concern. Large plasma current asymmetries (~10%) in JET disruptions are however observed only for short to moderate current quench times (up to 40 - 60ms, corresponding to 200 - 300ms in ITER if scaled with the plasma cross section area [50]) and the asymmetries are significantly smaller for longer quench times [51]. This implies that, at the ITER vessel resonance frequency, large asymmetries will only be able to complete a very small number of rotations, limiting the dynamic force amplification.

Disruption halo currents, convective heat loads and runaway electron generation can all be reduced by massive gas injection with the recently installed Disruption Mitigation Valve (DMV) using argon/deuterium and neon/deuterium gas mixtures [47]. Halo currents can be reduced by up to 60% provided the Thermal Quench (TQ) is initiated before a significant vertical movement has taken place. The peak heat loads during the thermal quench can be reduced by enhancing the radiation with MGI. In the cooling phase up to 50% of the thermal energy stored in the plasma before the DMV is activated is lost, predominantly by radiation before the TQ. About 40% of the remaining energy is radiated during the TQ. Thus, only 30% of the initial energy is lost by convection to plasma facing components during the TQ, only a small fraction of which is found in the divertor. For VDEs, which have the most peaked heat loads, the peak heat load on the upper dump plate can be reduced from 3.3MW/m^2 to 1.8MW/m^2 when MGI is employed [49].

Runaway electron generation is successfully avoided by the injection of Ar/D2 or Ne/D2 mixtures, due to the suppression of the Dreicer mechanism. In contrast, injection of pure Ar leads to runaway generation even at low toroidal magnetic fields. Although runaway electrons can be safely avoided by MGI in JET disruptions the density reached is still a factor 50 below the critical density for avalanche suppression which is essential in ITER where runaway currents of up to 10MA are expected due to the strong avalanche amplification. In order to keep forces on PFCs from eddy currents tolerable in ITER, the current decay time must stay above the lower bound of $\tau_{CQ} / S \approx 1.7$

ms/m^2 (with S the pre-disruption plasma cross-section area). This limit can be reached with pure Ar MGI in JET, whereas the deuterium mixtures show a slower current decay.

An extensive survey of all 2309 JET disruptions with $I_p > 1$ MA that occurred from 2000 to 2010 has allowed the sequences of events and root causes of the dominant classes of disruptions to be identified [48]. The dominant root cause of JET disruptions was found to be Neoclassical Tearing Modes (NTMs) that lead to locked modes, followed by human factors and density control problems, Fig. 10. More than half of all disruptions were caused by reasons other than pure physics instabilities, eg. subsystem failures (22%), control errors (15.8%), human errors (8.3%) or plasma-wall interactions (7.8%). Since the start of JET operations in 1983 the global disruptivity has decreased from ~20% to 3.4% thanks to increased operational experience and improved technical capabilities. About 0.4% of all JET disruptions are however caused by very fast and unpredictable events which may set a lower limit for the JET disruption rate.

5. ITER-RELEVANT ION CYCLOTRON RESONANCE HEATING STUDIES

Three ITER-relevant Ion Cyclotron Resonance Heating (ICRH) systems have been successfully tested on JET [52]; the ITER-Like Antenna (ILA) [53- 56] based on a similar design concept as the ITER ICRH antenna [57] with a closely packed array of short low inductance straps, two of the conventional "A2" antennas now equipped with External Conjugate-T (ECT) matching and two A2 antennas with 3dB hybrid couplers. All systems have demonstrated enhanced ELM resilience and have allowed up to 8.6 MW to be coupled on H-mode plasmas with Type I ELMs [17].

Most objectives of the ILA have been demonstrated; matching of an array of closely packed straps, ELM resilience using internal conjugate-T matching, arc detection using Scattering Matrix and Sub Harmonic Arc Detection (SMAD & SHAD) systems [58,59] and operation at ITER-relevant power densities (up to 6.2MW/m^2 on L-mode, 4.1MW/m^2 on H-mode) and RF voltages (42kV, also on ELMy H-mode plasmas). No evidence of increased impurity production has been found at these power densities which are up to 6 times higher than hitherto achieved on JET [55]. The main issue of concern for ITER was the low coupling (0.8 Ω/m) measured for the ILA on H-mode plasma with 5 cm strap to separatrix distance, lower than the originally anticipated 1.5 Ω/m. To assess the implications of the measured coupling for the coupling predictions made for ITER using RF codes such as TOPICA [60] a strap-separatrix distance scan with well-diagnosed L-mode edge density profiles was carried out and the coupling compared to TOPICA modelling. Good agreement for the effective strap resistance per unit length, R'_{eff}, and the effective conductance at the RF probe, G_{eff}, within the error bars was found, Fig. 11 [56]. This is in agreement with earlier TOPICA validation on Tore Supra [61], DIII-D [62] and Alcator-CMod [60] and, provided the edge density profiles used are realistic, gives confidence in the predictive capability of the code for ITER.

CONCLUSIONS AND OUTLOOK

Since the last IAEA Conference JET has made significant progress towards the qualification of ITER operating scenarios and the validation of ITER design choices and technologies. The exploitation of the ILW in the coming years will make JET the principal experiment for the development of

plasma scenarios compatible with the material combination foreseen for the active phase of ITER. The neutral beam power upgrade will allow stable H-mode operation at higher plasma currents and magnetic fields, allowing access to lower ρ^* and ν^* and higher β_N for reduced uncertainties in extrapolations to ITER. The increased pulse length will also be essential to progress the hybrid and steady state scenarios for ITER. This work is planned to lead up to a full deuterium-tritium campaign in the 2015 time frame for fully integrated tests of the Q=10 ITER baseline scenario, including the required active techniques for plasma-wall compatibility (impurity seeding, active ELM mitigation) in a metallic machine.

ACKNOWLEDGEMENTS

The results presented in this paper have been obtained by the collective efforts of all JET EFDA contributors, listed in the Appendix, and those working under the auspices of the JET Operation Contract. The authors are particularly thankful to M.N.A. Beurskens, E. de la Luna, P. de Vries, F. Durodié, W. Fundamenski, J. Graves, T.C. Hender, E. Joffrin, P.T. Lang, M. Lehnen, Y. Liang, J. Mailloux, D.C. McDonald, G. Saibene, R. Sartori, A.C.C. Sips and T. Tala. This work was supported by EURATOM and carried out within the framework of the European Fusion Development Agreement. The views and opinions expressed herein do not necessarily reflect those of the European Commission.

REFERENCES

[1]. F. Romanelli et al, Proc. 22nd IAEA FEC, Geneva, Switzerland, (2008)
[2]. ITER Physics Basis, Nucl. Fusion 39, 2368 (1999)
[3]. J. Paméla et al., J. Nucl. Mater., 363–365, 1–11 (2007)
[4]. V. Philipps, Ph. Mertens, G.F. Matthews, H. Maier et al., Fus. Eng. Des., in press
[5]. I. Nunes et al., this conference, EXC/P8-03
[6]. D. Ćirić et al., Fus. Eng. Des., 82, 610 (2007)
[7]. C. Ruset, E. Grigore, H. Maier, Phys. Scr. T128, 171-174 (2007)
[8]. C. Ruset et al., Proc. 26th Symposium on Fusion Technology, Porto, Portugal 2010
[9]. Ph. Mertens et al., Fus. Eng. Des., 84, 1289-1293 (2009)
[10]. Ph. Mertens et al., Proc. 26th Symposium on Fusion Technology, Porto, Portugal 2010
[11]. D.Ganuza et al., Fus. Eng. Des., 84, 810-814, (2009)
[12]. S. Shaw et al., Proc. 26th Symposium on Fusion Technology, Porto, Portugal 2010
[13]. F. Rimini et al., Proc. 26th Symposium on Fusion Technology, Porto, Portugal 2010
[14]. M.N.A. Beurskens et al., Plasma Phys. Control. Fusion 51, 124051 (2009)
[15]. T.H. Osborne et al., this conference, EXC/2-1
[16]. Fenstermacher et al., Nucl. Fusion 45, 1493-1502 (2005)
[17]. R. Sartori et al., this conference, EXC/P8-12
[18]. ITER Physics Basis, Nucl. Fusion 39, 2175 (1999)
[19]. E. Joffrin et al., this conference, EX/1-1
[20]. J. Mailloux et al., this conference, EXC/1-4

[21]. J. Garcia et al., Proc. 18th Topical Conf. on Radio Frequency Power in Plasmas, Gent, Belgium, (2009)
[22]. G. Giruzzi et al., this conference, FTP/P6-11
[23]. D. McDonald et al., this conference, EXC/2-4Rb
[24]. Y. Martin et al., J. Phys. Conf. Ser, 123, 012033 (2008)
[25]. W. Fundamenski et al., this conference, EXD/P3-11
[26]. G. Sips et al., this conference, EXC/P2-08
[27]. A.C. C. Sips et al., Nucl. Fusion 49, 085015 (2009)
[28]. P. Mantica et al., this conference, EXC/9-2
[29]. A.G. Peeters and D. Strintzi, Phys. Plasmas 11, 3748 (2004)
[30]. M. Kotschenreuther et al., Comput. Phys. Commun. 88, 128 (1995)
[31]. T. Tala et al., this conference, EXC/3-1
[32]. M.F.F.Nave et al., Phys. Rev. Lett. 105, 105005 (2010)
[33]. J. E. Rice et al., Nucl. Fusion 47, 1618 (2007)
[34]. J.P. Graves et al., this conference, THS/9-1
[35]. J.P. Graves et al. Phys. Rev. Lett. 102, 065005 (2009)
[36]. M. Laxåback et al., Nucl. Fusion 45, 1510 (2005)
[37]. E. de la Luna et al., this conference, EXC/8-4
[38]. Y. Liang et al., this conference, EXS/P3-04
[39]. P. Lang et al., this conference, EXS/P3-03
[40]. T. E. Evans et al., Nucl. Fusion 45, 595 (2005)
[41]. T. E. Evans et al., Nature Physics 2, 419 (2006)
[42]. Y. Liang et al., Phys. Rev. Lett. 105, 065001 (2010)
[43]. F. Köchl et al., Proc. 37th EPS Conf. On Plasma Physics, Dublin, Ireland, (2010)
[44]. T.Eich et al., Proc. 19th Int. Conf. on Plasma Surface Interactions, San Diego, USA, 2010
[45]. H. Thomsen et al., this conference, EXD/6-6Rb
[46]. T.C. Hender et al., this conference, EXS/10-3
[47]. M. Lehnen et al., this conference, EXS/P2-13
[48]. P. de Vries et al., this conference, EXS/P2-04
[49]. V. Riccardo et al., submitted to Plasma Phys. Controlled Fusion
[50]. ITER Physics Basis, Nucl. Fusion 39, 2137 (1999)
[51]. S. Gerasimov et al., Proc. 37th EPS Conf. on Plasma Physics, Dublin, Ireland, (2010)
[52]. F. Durodie et al., this conference, EXW/P7-04
[53]. F. Durodié et al., in Radio Frequency Power in Plasmas, AIP Conf. Proceedings 595, 122 (2001)
[54]. F. Durodié et al., Fus. Eng. Des. 74, 223 (2005)
[55]. F. Durodié et al., in RF Power in Plasmas, AIP Conf. Proc. 1187, 221-224 (2009)
[56]. M.P.S. Nightingale et al., in RF Power in Plasmas, AIP Conf. Proc. **1187**, 213-220 (2009)
[57]. D. Bora et al., 17th Topical Conf. on Radio Frequency Power in Plasmas, Clearwater, Florida, AIP Conf. Proceedings 933, 25-32 (2007)

[58]. M. Vrancken et al., Proc. 26th Symposium on Fusion Technology, Porto, Portugal 2010
[59]. P. Jacquet, et al., in RF Power in Plasmas, AIP Conf. Proc. 1187, 241-244 (2009)
[60]. V. Lancellotti et al., Nucl. Fusion 46, S476 (2006)
[61]. D. Milanesio et al., Plasma Phys. Controlled Fusion 49, 405 (2007)
[62]. R. Maggiora et al., Nucl. Fusion 44, 846 (2004)

Appendix: List of JET EFDA Contributors

I. Abel[1], V. Afanesyev[2], G. Agarici[3], K.M. Aggarwal[4], M. Airila[5], R. Akers[6], Th. Alarcon[3], R. Albanese[7], A. Alexeev[8], A. Alfier[9], P. Allan[6], S. Almaviva[10], A. Alonso[11], M. Alonso[12], B. Alper[6], H. Altmann[6], D. Alves[12], G. Ambrosino[7], V. Amosov[8], G. Anda[13], F. Andersson[14], E. Andersson Sundén[15], V. Andreev[16], Y. Andrew[6], M. Angelone[17], M. Anghel[18], A. Anghel[19], C. Angioni[20], G. Apruzzese[17], N. Arcis[6], P. Arena[21], A. Argouarch[3], M. Ariola[7], A. Armitano[3], R. Armstrong[22], G. Arnoux[6], S. Arshad[23], G. Artaserse[7], J.F. Artaud[3], A. Ash[6], E. Asp[24,15], O. Asunta[25], C.V. Atanasiu[19], G. Atkins[6], M.D. Axton[6], C. Ayres[6], A. Baciero[11], V. Bailescu[26], B. Baiocchi[27], R.A. Baker[6], I. Balboa[6], C. Balorin[3], N. Balshaw[6], J.W. Banks[6], Y.F. Baranov[6], D. Barbier[3,24], I.L. Barlow[6], M.A. Barnard[6], R. Barnsley[4], L. Barrena[11], L. Barrera[11], M. Baruzzo[9], V. Basiuk[3], G. Bateman[28], P. Batistoni[17], N. Baumgarten[29], L. Baylor[30], B. Bazylev[31], P.S. Beaumont[6], K. Beausang[22], M. Bécoulet[3], N. Bekris[31], M. Beldishevski[6], A.C. Bell[6], F. Belli[17], M. Bellinger[6], T. Bellizio[7], P.S.A. Belo[12], É. Belonohy[20], P.E. Bennett[6], N.A. Benterman[6], G. Berger-By[3], H. Bergsåker[32], H. Berk[33], J. Bernardo[12], B. Bertrand[3], M.N.A. Beurskens[6], B. Bieg[34], B. Bienkowska[34], T. Biewer[30], T.M. Biewer[30], M. Bigi[9], R. Bilato[20], J. Bird[6], J. Bizarro[12], T.R. Blackman[6], P. Blanchard[35,24], E. Blanco[11], J. Blum[36], V. Bobkov[20], A. Boboc[6], D. Boilson[22], I. Bolshakova[37], T. Bolzonella[9], L. Boncagni[17], G. Bonheure[38], X. Bonnin[3], D. Borba[39,12], A. Borthwick[6], A. Botrugno[17], C. Boulbe[36], F. Bouquey[3], C. Bourdelle[3], K.v. Bovert[29], M. Bowden[6], T. Boyce[6], H.J. Boyer[6], A. Bozhenkov[29], R.J. Brade[6], J.M.A. Bradshaw[6], J. Braet[40], V. Braic[41], G.C. Braithwaite[6], C. Brault[3], H. Braune[42], B. Breizman[33], S. Bremond[3], P.D. Brennan[6], A. Brett[6], J. Breue[43], S. Brezinsek[29], M.D.J. Bright[6], F. Briscoe[6], M. Brix[6], M. Brombin[9], B.C. Brown[6], D.P.D. Brown[6], A. Bruschi[27], J. Brzozowski[32], J. Bucalossi[3], M.A. Buckley[6], T. Budd[6], R. Budny[44], R.V. Budny[44], P. Bunting[6], P. Buratti[17], G. Burcea[26], P.R. Butcher[6], R.J. Buttery[45], R. Cação[12], G. Calabrò[17], C.P. Callaghan[6], J.P. Caminade[3], P.G. Camp[6], D.C. Campling[6], J. Canik[30], B. Cannas[46], A.J. Capel[6], G. Carannante[7], P.J. Card[6], A. Cardinali[17], T. Carlstrom[45], P. Carman[6], D. Carralero[11], L. Carraro[9], T. Carter[47], B.B. Carvalho[12], P. Carvalho[12], A. Casati[3], C. Castaldo[17], J. Caughman[30], R. Cavazzana[9], M. Cavinato[9], M. Cecconello[15], F.E. Cecil[48], A. Cenedese[9], C. Centioli[17], R. Cesario[17], C.D. Challis[6], M. Chandler[6], C. Chang[49], A. Chankin[20], I.T. Chapman[6], D.J. Child[6], P. Chiru[19], G. Chitarin[9], I. Chugonov[2], I. Chugunov[2], D. Ciric[6], F. Clairet[3], R.H. Clarke[6], R. Clay[6], M. Clever[29], J.P. Coad[6], P.A. Coates[6], V. Coccorese[7], V. Cocilovo[17], S. Coda[35], R. Coelho[12], J. Coenen[29], I. Coffey[4], L. Colas[3], M. Cole[30], S. Collins[6], S. Combs[30], J. Compan[43], J.E. Conboy[6], S. Conroy[15], N. Cook[6], S.P. Cook[6], D. Coombs[6], S.R. Cooper[6], Y. Corre[3], G. Corrigan[6], S. Cortes[12], D. Coster[20], G.F. Counsell[6], X. Courtois[3], M. Cox[6], T. Craciunescu[19], S. Cramp[6], F. Crisanti[17], O. Croft[6], K. Crombe[50], B.J. Crowley[6], N. Cruz[12], L. Cupido[12], M. Curuia[18], R.A. Cusack[6], A. Czarnecka[34], S. Dalley[6], E.T. Daly[6], A. Dalziel[6], D. Darrow[44], O. David[51], N. Davies[6], J.J. Davis[6], I.E. Day[6], C. Day[31], R. De Angelis[17], G. de Arcas[52], M.R. de Baar[53], E. de la Cal[11], E. de la Luna[11,24], J.L. de Pablos[11], G. De Temmerman[35], G. De Tommasi[7], P.C. de Vries[53], R. De-Angelis[17], F. Degli Agostini[9], E. Delabie[53], D. del-Castillo-Negrete[30], L. Delpech[3], G. Denisov[54], A.J. Denyer[6], R.F. Denyer[6], S. Devaux[20], P. Devynck[3], L. Di Matteo[17], L. Di Pace[17], P.J. Dirken[6], A. Dnestrovskiy[16], D. Dodt[20], K. Dominiczak[43], S.E. Dorling[6], D. Douai[3], A.P. Down[6], P.T. Doyle[6], J.R. Drake[32], T. Dreischuh[55], V. Drozdov[6], P. Dumortier[38], D. Dunai[13], I. Duran[56], F. Durodié[38], K. Dylst[40], R. Eaton[6], T. Edlington[6], A.M. Edwards[6], D.T. Edwards[6], P.K. Edwards[6], Th. Eich[20], A. Ekedahl[3], T. Elevant[32], A. Elfimov[12], B. Ellingboe[22], C.G. Elsmore[6], B. Emmoth[57], G. Ericsson[15], L.G. Eriksson[58], A. Eriksson[14], B. Esposito[17], H.G. Esser[29], T. Estrada[11], E.A. Evangelidis[59], G.E. Evans[6], G.D. Ewart[6], D.T. Ewers[6], G. Falchetto[3], D. Falie[19], J.G.A. Fanthome[6], D. Farina[27], J.W. Farthing[6],

A. Fasoli[35], B. Faugeras[36], N. Fedorczak[3], R.C. Felton[6], C. Fenzi[3], H. Fernandes[12], J.A. Ferreira[11], J. Ferreira[12], J. Ferron[45], J.A. Fessey[6], L. Figini[27], A. Figueiredo[12], J. Figueiredo[12], P. Finburg[6], K.H. Finken[29], U. Fischer[31], N. Fitzgerald[22], J. Flanagan[6], C. Fleming[6], A. Fonseca[12], A.D. Forbes[6], O. Ford[1], A. Formisano[7], D. Fraboulet[3], R.J. Francis[6], L. Frassinetti[32], R. Fresa[7], J.P. Friconneau[51], D. Frigione[17], J.C. Fuchs[20], K. Fullard[6], W. Fundamenski[6], M. Furno Palumbo[7], J. Gafert[20], K. Gál[13], R. Galvão[12], S. Garavaglia[27], X. Garbet[3], J. Garcia[3], M. Garcia Munoz[20], W. Gardner[30], P. Garibaldi[3], D. Garnier[3], L. Garzotti[6], M. Gatu Johnson[15], P. Gaudio[10], E. Gauthier[3], J.W. Gaze[6], D.F. Gear[6], J. Gedney[6], S.J. Gee[6], M. Gelfusa[10], E. Genangeli[24,17], S. Gerasimov[6], A. Geraud[3], T. Gerbaud[3], M. Gherendi[19], N. Ghirelli[3], J.C. Giacalone[3], L. Giacomelli[60], C.S. Gibson[6], C. Gil[3], S.J. Gilligan[6], C.G. Gimblett[6], D. Gin[2], E. Giovannozzi[17], C. Giroud[6], G. Giruzzi[3], S. Glowacz[34], J. Godwin[6], J.K. Goff[6], P. Gohil[45], V. Goloborod'ko[61], B. Gonçalves[12], M. Goniche[3], S. Gonzales[11], S.M. González de Vicente[40], A. Goodyear[6], N. Gorelenkov[44], G. Gorini[27], R. Goulding[30], B. Graham[6], D. Graham[6], M.E. Graham[6], G. Granucci[27], J. Graves[35], N.R. Green[6], H. Greuner[20], E. Grigore[19], F.S. Griph[6], C. Grisolia[3], G. Gros[3], G. Grossetti[27], M. Groth[25], S. Grünhagen[6], M.P. Gryaznevich[6], R. Guirlet[3], B. Gulejova[35], J. Gunn[3], A. Gupta[29], P. Guzdar[62], P. Hacek[56], L.J. Hackett[6], S. Hacquin[3], B. Haist[6], A. Hakola[25], S.J. Hall[6], S.P. Hallworth Cook[6], D.T. Hamilton[6], H. Han[63], R.C. Handley[6], S. Harding[6], J.D.W. Harling[6], D. Harting[29], M.J. Harvey[6], T.D.V. Haupt[6], E. Havlickova[56], N.C. Hawkes[6], R. Hawryluk[44], J.H. Hay[6], N. Hayashi[49], P.W. Haydon[6], I.R. Hayward[6], S. Hazel[6], P.J.L. Heesterman[6], W. Heidbrink[44], J. Heikkinen[5], C. Hellesen[15], T. Hellsten[32], O.N. Hemming[6], T.C. Hender[6], M. Henderson[64], C. Hennig[20], V. Hennion[3], C. Hidalgo[11], S. Higashijima[49], J.W. Hill[6], M. Hill[6], K. Hill[44], J. Hillairet[3], D. Hillis[30], T. Hirai[43], M. Hitchin[6], J. Hobirk[20], C. Hogan[30], C.H.A. Hogben[6], G.M.D. Hogeweij[53], I.C. Hollingham[6], R. Holyaka[37], D.A. Homfray[6], G. Honeyands[6], S.H. Hong[3], C. Hopf[20], B.A. Horn[6], A.R. Horton[6], L.D. Horton[24,58], S.P. Hotchin[6], M.R. Hough[6], W. Houlberg[30], D.F. Howell[6], M. Hron[56], A. Huber[29], T.M. Huddleston[6], Z. Hudson[6], M. Hughes[6], M. Hühnerbein[43], C.C. Hume[6], A.J. Hunt[6], C.L. Hunter[6], T.S. Hutchinson[6], S. Huygen[38], G. Huysmans[3], V. Hynönen[25], S. Ide[49], R. Igreja[12], C. Illescas[11], F. Imbeaux[3], D. Ivanova[32], E. Ivings[6], S. Jachmich[38], G. Jackson[45], P. Jacquet[6], K. Jakubowska[34], M. Jakubowski[42], P.V. James[6], R.J.E. Jaspers[53], S. Jednorog[34], I. Jenkins[6], M.A.C. Jennison[6], C. Jeskins[6], O. Jin Kwon[65], E. Joffrin[3,24], M.F. Johnson[6], R. Johnson[6], T. Johnson[32], D. Jolovic[29], V. Jonauskas[66], E.M. Jones[6], G. Jones[6], H.D. Jones[6], T.T.C. Jones[6], M. Jouvet[3], C. Jupén[67], I. Kachtchouk[8], J. Kaczmarczyk[34], A. Kallenbach[20], J. Källne[68], D. Kalupin[29], S. Kálvin[13], G. Kamelander[61], R. Kamendje[69], A. Kappatou[70], S. Karttunen[5], W. Kasparek[71], I. Katramados[6], M. Kaufmann[20], G. Kaveney[6], A.S. Kaye[6], M.J. Kear[6], D.L. Keeling[6], D. Kelliher[22], M. Kempenaars[6], P. Khilar[6], N.G. Kidd[6], M. Kiisk[72], K.M. Kim[63], R.F. King[6], D.J. Kinna[6], V. Kiptily[6], G. Kirnev[16], N. Kirneva[16], K. Kirov[6], A. Kirschner[29], R. Kisielius[66], D. Kislov[16], G. Kiss[29], T. Kiviniemi[25], G. Kizane[73], A. Klein[74], A. Klix[31], M. Knaup[29], K. Kneuper[6], H. Kneupner[29], P.J. Knight[6], S.J. Knipe[6], M. Kocan[3], F. Köchl[61], G. Kocsis[13], C. Konz[20], T. Koppitz[43], A. Korotkov[6], H.R. Koslowski[29], V. Kotov[29], M.D. Kovari[6], K. Kovarik[56], G. Kramer[44], A. Krasilnikov[8], V. Krasilnikov[8], S. Kraus[29], A. Kreter[29], K. Krieger[20], A. Kritz[28], Y. Krivchenkov[6], U. Kruezi[29], M. Krychowiak[42], S. Krylov[16], I. Ksiazek[34], M. Kubic[56], S. Kuhn[61], W. Kühnlein[43], T. Kurki-Suonio[25], A. Kurowski[34], B. Kuteev[16], A. Kuyanov[16], R. La Haye[45], M. Laan[72], C. Labate[7], A. Lachichi[6], N. Lam[6], P. Lang[20], M.T. Large[6], I. Lassiwe[29], J.R. Last[6], K.D. Lawson[6], M. Laxåback[24,32], R.A. Layne[6], E. Lazzaro[27], F. Le Guern[3], B. LeBlanc[44], H.J. Leggate[22], M. Lehnen[29], M. Leigheb[17], I. Lengar[75], M. Lennholm[24,58], E. Lerche[38], C.N. Lescure[6], Y. Li[74], A. Li Puma[3], Y. Liang[29], J. Likonen[5], Y. Lin[74], J. Linke[43], S.A. Linstead[6], B. Lipshultz[74], X. Litaudon[3], A.G. Litvak[54], Y. Liu[6],

T. Loarer[3], A. Loarte[64], R.C. Lobel[6], P.J. Lomas[6], F.D. Long[6], J. Lönnroth[25], D.J. Looker[6], J. Lopez[11], Ph. Lotte[3], M.J. Loughlin[6], A.B. Loving[6], C. Lowry[24,58], T. Luce[45], R.M.A. Lucock[6], A. Lukanitsa[76], A.M. Lungu[19], C.P. Lungu[19], A. Lyssoivan[38], P. Macheta[6], A.S. Mackenzie[6], M. Macrae[6], G. Maddaluno[17], G.P. Maddison[6], J. Madsen[77], P. Maget[3], C. Maggi[20], H. Maier[20], J. Mailloux[6], M. Makowski[45], C.J. Manning[6], M. Mansfield[22], M.E. Manso[12], P. Mantica[27], M. Mantsinen[25], M. Maraschek[20], C. Marchetto[27], M.A. Marchitti[7], M. Mardenfeld[44], J.L. Marechal[3], M. Marinelli[10], A. Marinoni[35], M. Marinucci[17], J. Märki[35], D. Marocco[17], C.A. Marren[6], D. Martin[6], D.L. Martin[6], G. Martin[3], Y. Martin[35], J.R. Martín-Solís[78], K. Masaki[49], A. Masiello[9], M. Maslov[35], C. Maszl[61], A. Matilal[6], M. Mattei[7], G.F. Matthews[6], F. Maviglia[7], C.R. May[6], M. Mayer[20], M.L. Mayoral[6], D. Mazon[3], C. Mazzotta[17], E. Mazzucato[44], P. McCarthy[22], K.G. McClements[6], K. McCormick[20], P.A. McCullen[6], D. McCune[44], D.C. McDonald[6], R. Mcgregor[6], J.P. Mckivitt[6], A. Meakins[6], F. Medina[11], A.G. Meigs[6], M. Menard[45], L. Meneses[12], S. Menmuir[79], I.R. Merrigan[6], Ph. Mertens[29], A. Messiaen[38], H. Meyer[6], G. Miano[7], M. Miele[7], P. Migliucci[10], A.G. Miller[6], S.F. Mills[6], J.J. Milnes[6], K. Min Kim[63], T. Mindham[6], F. Mirizzi[17], E. Mirones[11], M. Mironov[2], R. Mitteau[3], J. Mlynar[56], P. Mollard[3], I. Monakhov[6], P. Monier-Garbet[3], R. Mooney[6], S. Moradi[80], D. Moreau[3], Ph. Moreau[3], L. Moreira[6], A. Morgan[6], P.D. Morgan[6], C. Morlock[24,29], A. Moro[27], A.W. Morris[6], G.L. Mort[6], C. Mrozek[20], A. Mueck[35], H.W. Müller[20], M. Murakami[30], A. Murari[24,9], I. Mustata[19], F. Nabais[12], E. Nardon[3], G. Nash[6], V. Naulin[77], M.F.F. Nave[12], R. Nazikian[44], I. Nedzelski[12], C.R. Negus[6], J.D. Neilson[6], A. Neto[12], R. Neu[20], O. Neubauer[29], G.J. Newbert[6], M. Newman[6], K.J. Nicholls[6], A. Nicolai[29], L. Nicolas[3], P. Nieckchen[24,20], P. Nielsen[9], A.H. Nielsen[77], S.K. Nielsen[77], G. Nielson[44], J. Nieto[52], M.P.S. Nightingale[6], C. Noble[6], M. Nocente[27], M. Nora[25], H. Nordman[14], M. Norman[6], J-M. Noterdaeme[20], S. Nowak[27], I. Nunes[24,12], F. Ognissanto[27], T. O'Gorman[22], S. Olariu[81], A. Oleynikov[8], M. O'Mullane[82], J. Ongena[38], F. Orsitto[17], O.I. Oswuigwe[6], M. Ottaviani[3], N. Oyama[49], D. Pacella[17], K. Paget[6], S. Palazzo[21], J. Pamela[3], S. Pamela[3], R. Panek[56], L. Pangione[6], A. Panin[29], Th. Panis[35], A. Pankin[28], A. Pantea[19], V. Parail[6], Th. Parisot[3], A. Parkin[6], A. Parsloe[6], B.T. Parsons[6], R. Pasqualotto[9], P. Pastor[3], R. Paterson[6], M.K. Paul[29], D. Peach[6], R.J.H. Pearce[6], B.J. Pearson[6], I.J. Pearson[6], L.C. Pedrick[6], M.A. Pedrosa[11], B. Pegourie[3], R. Pereira[12], E. Perelli Cippo[27], G. Pereverzev[20], A. Perevezentsev[6], Ch. Perez von Thun[24,20], V. Pericoli-Ridolfini[39,17], A. Perona[83], Y. Perrot[51], S. Peruzzo[9], S. Peschanyy[31], G. Petravich[13], L. Petrizzi[17], V. Petrov[8], V. Petrzilka[56], V. Philipps[29], G. Piazza[31], F. Piccolo[6], A. Pietropaolo[27], M. Pillon[17], S.D. Pinches[6], T. Pinna[17], G. Pintsuk[43], P. Piovesan[9], A. Pironti[7], F. Pisano[46], R. Pitts[64], B. Plaum[71], V. Plyusnin[12], M. Polasik[34], F.M. Poli[84], N. Pomaro[9], O. Pompilian[19], L. Poncet[3], P.J. Pool[6], S. Popovichev[6], F. Porcelli[83], M.T. Porfiri[17], C. Portafaix[3], A. Pospieszczyk[29], G. Possnert[68], G. Prestopino[10], P. Prior[6], R. Prokopowicz[34], I. Proverbio[27], R. Pugno[20], M.E. Puiatti[9], K. Purahoo[6], V. Pustovitov[16], Th. Pütterich[20], D. Püttmann-Kneupner[29], A. Quercia[7], E. Rachlew[79], R. Rademaker[53,24], T. Rafiq[28], M.S.J. Rainford[6], G. Ramogida[17], K. Rantamäki[5], J. Rapp[29], J.J. Rasmussen[77], G. Rattá[11], G. Ravera[17], M. Reich[20], R. Reichle[3], D. Reiser[29], R. Reiss[3], D. Reiter[29], D. Rendell[6], C. Reux[3], G. Rewoldt[74], T.T. Ribeiro[12], V. Riccardo[6], D. Richards[6], F. Rigollet[3], F.G. Rimini[24,58], L. Rios[11], M. Riva[17], J.E.C. Roberts[6], R.J. Robins[6], D.S. Robinson[6], S.A. Robinson[6], D.W. Robson[6], H. Roche[3], M. Rödig[43], N. Rodionov[8], V. Rohde[20], A. Rolfe[6], M. Romanelli[6], F. Romanelli[24,17], A. Romano[17], J. Romero[11], E. Ronchi[15], S. Rosanvallon[3], Ch. Roux[3], S. Rowe[6], M. Rubel[32], G. Rubinacci[7], L. Ruchko[12], M. Ruiz[52], C. Ruset[19], M. Russell[6], A. Ruth[22], L. Ryc[34], A. Rydzy[17], F. Ryter[20], J. Rzadkiewicz[34], S. Saarelma[6], F. Sabathier[3], R. Sabot[3], S. Sadakov[29], P. Sagar[6], G. Saibene[23], A. Saille[3], F. Saint-Laurent[3], A. Salmi[25], R. Salomaa[25], F. Salzedas[12], U. Samm[29], P. Sanchez[11], S. Sanders[6], S.G. Sanders[6], G. Sandford[6], K. Sandland[6], P. Sandquist[14], D.E.G. Sands[6], M.I.K. Santala[25], F. Sartori[23], R. Sartori[23], O. Sauter[35],

A. Savelyev[2], A. Savtchkov[29], S.C. Scales[6], A. Scarabosio[20], N. Schaefer[3], Ch. Schlatter[35], V. Schmidt[9], A. Schmidt[29], O. Schmitz[29], S. Schmuck[42], M. Schneider[3], M. Scholz[34], K. Schöpf[61], B. Schweer[29], J. Schweinzer[20], B. Scott[20], M. Seki[49], L. Semeraro[17], A. Semerok[85], G. Sergienko[29], F. Serra[12], M. Sertoli[20], M.M.J. Shannon[6], S.E. Sharapov[6], S.R. Shaw[6], A. Shevelev[2], R. Sievering[43], C.A. Silva[12], P.A. Simmons[6], A. Simonetto[27], D. Simpson[6], S. Sipila[25], A.C.C. Sips[24,58], A. Sirinelli[6], H. Sjöstrand[15], D. Skopintsev[8], K. Slabkowska.[34], P.G. Smith[6], J. Snipes[74], L. Snoj[75], S. Snyder[28], S. Soare[18], E.R. Solano[11], S. Soldatov[38], A. Soleto[11], W. Solomon[44], C. Soltane[3,24], P. Sonato[9], A. Sopplesa[9], A. Sorrentino[7], J. Sousa[12], C.B.C. Sowden[6], C. Sozzi[27], P. Späh[31], T. Spelzini[6], J. Spence[6], F. Spineanu[19], P. Spuig[3], A. Stäbler[20], R.D. Stagg[6], M.F. Stamp[6], V. Stancalie[19], P. Stangeby[45], C. Stan-Sion[81], D.E. Starkey[6], M.J. Stead[6], A.V. Stephen[6], A.L. Stevens[6], J. Stober[20], R.B. Stokes[6], D. Stork[6], D. Stoyanov[55], J. Strachan[44], P. Strand[14], M. Stransky[14], D. Strauss[31], D. Strintzi[70], W. Studholme[6], Y. Su Na[63], F. Subba[83], H.P. Summers[82], Y. Sun[29], C. Surdu-Bob[19], E. Surrey[6], D.J. Sutton[6], J. Svensson[20], D. Swain[30], B.D. Syme[6], I.D. Symonds[6], T. Szepesi[13], A. Szydlowski[34], F. Tabares[11], V. Takalo[86], H. Takenaga[49], T. Tala[5], A.R. Talbot[6], C. Taliercio[9], C. Tame[6], G. Tardini[20], M. Tardocchi[27], L. Taroni[9], G. Telesca[38], A. Terra[29], A.O. Terrington[6], D. Testa[35], J.M. Theis[3], J.D. Thomas[6], P.D. Thomas[6], P.R. Thomas[23], V.K. Thompson[6], H. Thomsen[20], C. Thomser[29], A. Thyagaraja[6], P.A. Tigwell[6], I. Tiseanu[19], R. Tivey[24,58], J.M. Todd[6], T.N. Todd[6], M.Z. Tokar[29], S. Tosti[17], P. Trabuc[3], J.M. Travere[3], W. Treutterer[20], P. Trimble[6], A. Trkov[75], E. Trukhina[16], M. Tsalas[24,59], H. Tsige-Tamirat[31], E. Tsitrone[3], D. Tskhakaya jun[61], O. Tudisco[17], S. Tugarinov[8], M.M. Turner[22], G. Turri[35], S.G.J. Tyrrell[6], N. Umeda[49], B. Unterberg[29], H. Urano[49], A.J. Urquhart[6], I. Uytdenhouwen[40], A. Vaccaro[31], A.P. Vadgama[6], G. Vagliasindi[17], D. Valcarcel[12], M. Valisa[9], J. Vallory[3], M. Valovic[6], D. Van Eester[38], B. van Milligen[11], G.J. van Rooij[53], C.A.F. Varandas[12], S. Vartanian[3], V. Vdovin[16], J. Vega[11], G. Verdoolaege[87], J.M. Verger[3], L. Vermare[3], C. Verona[10], Th. Versloot[53], M. Vervier[38], J. Vicente[12], S. Villari[17], E. Villedieu[3], F. Villone[7], J.E. Vince[6], G.J. Vine[6], B. Viola[7], E. Vitale[17], R. Vitelli[10], M. Vlad[19], I. Voitsekhovitch[6], M. Vrancken[38], K. Vulliez[3], C.W.F. Waldon[6], M. Walker[6], M.J. Walsh[6], J. Waterhouse[6], M.L. Watkins[6,24], M.J. Watson[6], T. Wauters[3], M.W. Way[6], C.R. Webb[6], J. Weiland[14], H. Weisen[35,24], M. Weiszflog[15], R. Wenninger[20], A.T. West[6], J.M. Weulersse[85], B. Weyssow[80,39], M.R. Wheatley[6], A.D. Whiteford[82], A.M. Whitehead[6], A.G. Whitehurst[6], A.M. Widdowson[6], R.C. Wieggers[53], C. Wiegmann[29], S. Wiesen[29], A. Wilson[6], D. Wilson[6], D.J. Wilson[6], H.R. Wilson[88], M. Wischmeier[20], D.M. Witts[6], R.C. Wolf[29], J. Wolowski[34], P. Woscov[74], G.M. Wright[53], J. Wright[74], G.S. Xu[89], V. Yavorskij[61], V. Yerashok[37], J. Yorkshades[6], C. Young[6], D. Young[6], I.D. Young[6], X. Yuhong[38], L. Zabeo[6], A. Zabolotsky[35], L. Zaccarian[17], R. Zagorski[39,34], F.S. Zaitsev[76], S. Zajac[34], L. Zakharov[44], R. Zanino[83], V. Zaroschi[19], K.D. Zastrow[6], I. Zatz[44], B. Zefran[75], W. Zeidner[20], M. Zerbini[17], T. Zhang[29], Y. Zhu[89], E. Zilli[27], O. Zimmermann[29], V. Zoita[24,19], S. Zoletnik[13], W. Zwingman[3]

1. Imperial College, University of London, London, SW7 2AZ, UK
2. Ioffe Physico-Technical Institute, 26 Politekhnicheskaya, St Petersburg 194021, Russia Federation
3. Association EURATOM-CEA, CEA/DSM/IRFM, Cadarache 13108 Saint Paul Lez Durance, France
4. Department of Pure and Applied Physics, Queens University, Belfast, BT7 1NN, UK
5. VTT Technical Research Centre of Finland, Association EURATOM-Tekes, P.O.Box 1000, FIN-02044 VTT, Finland
6. Euratom/CCFE Fusion Association, Culham Science Centre, Abingdon, Oxon, OX14 3DB, UK
7. Associazione EURATOM-ENEA sulla Fusione, Consorzio CREATE, Via Claudio 21, 80125 Napoli, Italy
8. Troitsk Insitute of Innovating and Thermonuclear Research (TRINITI), Troitsk 142190, Moscow Region, Russian Federation
9. Associazione EURATOM-ENEA sulla Fusione, Consorzio RFX Padova, Italy
10. Associazione EURATOM-ENEA sulla Fusione, Università di Roma, Italy
11. Laboratorio Nacional de Fusion, Asociacion EURATOM-CIEMAT, Madrid, Spain
12. Associação EURATOM/IST, Instituto de Plasmas e Fusão Nuclear, Instituto Superior Técnico, Av Rovisco Pais, 1049-001 Lisbon, Portugal
13. KFKI-Research Institute for Particle and Nuclear Physics, Association EURATOM, P.O.Box 49, H-1525, Budapest, Hungary
14. Association EURATOM-VR, Department of Earth and Space Sciences, Chalmers University of Technology, SE-41296 Gothenburg, Sweden
15. Association EURATOM-VR, Department of Physics and Astronomy, Uppsala University, SE-75120 Uppsala, Sweden
16. RRC Kurchatov Institute, 1 Kurchatov Square, Moscow 123182, Russian Federation
17. Associazione EURATOM-ENEA sulla Fusione, C.R. Frascati, Roma, Italy
18. The National Institute for Cryogenics and Isotopic Technology, Association EURATOM-MEdC, Ramnicu Valcea, Romania
19. The National Institute for Laser, Plasma and Radiation Physics, Association EURATOM-MEdC, Magurele-Bucharest, Romania
20. Max-Planck-Institut für Plasmaphysik, EURATOM-Assoziation, D-85748 Garching, Germany
21. Dipartimento di Ingegneria Elettrica Elettronica e dei Sistemi-Università degli Studi di Catania, 95125 Catania, Italy
22. Dublin City University (DCU), Ireland
23. Fusion for Energy Joint Undertaking, Josep Pl. 2, Torres Diagonal Litoral B3, 08019, Barcelona, Spain
24. EFDA Close Support Unit, Culham Science Centre, Culham, OX14 3DB, UK
25. Aalto University, Association EURATOM-Tekes, P.O.Box 14100, FIN-00076 Aalto, Finland
26. The Nuclear Fuel Plant, Pitesti, Romania
27. Associazione EURATOM-ENEA sulla Fusione, IFP Milano, Italy
28. Lehigh University, Bethlehem, PA 18015, Pennsylvania, USA
29. Forschungszentrum Jülich, Institute of Energy Research - Plasma Physics, EURATOM Association, D-52425, Jülich, Germany
30. Oak Ridge National Laboratory, Oak Ridge, TN 37831-6169, Tennessee, USA

31. Karlsruhe Institute of Technology, P.O.Box 3640, D-76021 Karlsruhe, Germany
32. Association EURATOM-VR, Fusion Plasma Physics, EES, KTH, SE-10044 Stockholm, Sweden
33. University of Texas at Austin, Institute for Fusion Studies, Austin, TX 78712, Texas, USA
34. Association Euratom-IPPLM, Hery 23, 01-497 Warsaw, Poland
35. Association EURATOM-Confédération Suisse, Ecole Polytechnique Fédérale de Lausanne (EPFL), CRPP, CH-1015 Lausanne, Switzerland
36. Laboratoire J.A.Dieudonné, Université de Nice-Sophia-Antipolis, Parc Valrose, F-06108 Nice CE DEX 02, France
37. Magnetic Sensor Laboratory (LPNU), 1 Kotliarevsky Str, Lviv, 79013, Ukraine
38. Association "EURATOM - Belgian State" Laboratory for Plasma Physics Koninklijke Militaire School-Ecole Royale Militaire Renaissancelaan 30 Avenue de la Renaissance B-1000 Brussels Belgium
39. EFDA Close Support Unit, D-85748 Garching, Germany
40. Association EURATOM-SCK-CEN, Nuclear Research Centre, 2400 Mol, Belgium
41. The National Institute for Optoelectronics, Magurele-Bucharest, Romania, Association EURATOM-MEdC
42. Max-Planck-Institut für Plasmaphysik, Teilinsitut Greifswald, EURATOM-Assoziation, D-17491 Greifswald, Germany
43. Forschungszentrum Jülich, Institute of Energy Research, EURATOM Association, D-52425, Jülich, Germany
44. Princeton Plasma Physics Laboratory, James Forrestal Campus, Princeton, NJ 08543, New Jersey, USA
45. General Atomics, P.O.Box 85608, San Diego, CA 92186-5608, California, USA
46. Department of Electrical and Electronic Engineering, University of Cagliari, Piazza d'Armi 09123 Cagliari, Italy
47. University of California, 1111 Franklin St., Oakland, CA 94607, USA
48. Colorado School of Mines, 1500 Illinois Street, Golden, CO 80401, Colorado, USA
49. Japan Atomic Energy Agency, Naka Fusion Research Establishment, Nakamachi, Naka-gun, Ibaraki-ken 311-0913, Japan
50. Department of Applied Physics UG (Ghent University) Rozier 44 B-9000 Ghent Belgium
51. CEA/Fontenay aux Roses, B.P.6 F-92265 Fontenay-aux-roses CEDEX, France
52. Universidad Politécnica de Madrid, Grupo I2A2, Madrid, Spain
53. FOM Institute for Plasma Physics Rijnhuizen, Association EURATOM-FOM, Trilateral Euregio Cluster, The Netherlands
54. Institute of Applied Physics, Nizhny Novgorod 603155, Russian Federation
55. Bulgarian Academy of Sciences, 6 Moskovsak Str., Sofia 1000, Bulgaria
56. Association EURATOM-IPP.CR, Institute of Plasma Physics AS CR, Za Slovankou 3, 182 21 Praha 8, Czech Republic
57. Association EURATOM-VR, Department of Material Physics, ICT, KTH, SE-16440 Kista, Sweden
58. European Commission, B-1049 Brussels, Belgium
59. Association EURATOM-Hellenic Republic, NCSR "Demokritos" 153 10, Agia Paraskevi Attikis, Greece

60. Physikalisch-Technische Bundesanstalt, Bundesallee 100, D-38116, Braunschweig, Germany
61. Association EURATOM-Österreichische Akademie der Wissenschaften (ÖAW), Austria
62. Institute for Plasma Research, University of Maryland, College Park, MD 20742-3511, Maryland, USA
63. Seoul National University, Shilim-Dong, Gwanak-Gu, Republic of Korea
64. ITER Organization, Route de Vinon, CS 90 046, 13067 Saint Paul Lez Durance, France
65. Daegu University, Jillyang, Gyeongsan, Gyeongbuk 712-174, Republic of Korea
66. Association EURATOM-LEI, Breslaujos str. 3, LT-44403, Kaunas, Lithuania
67. Association EURATOM-VR, Department of Physics, Lund University, SE-22100 Lund, Sweden
68. Association EURATOM-VR, Department of Engineering Sciences, Uppsala University, SE-75120 Uppsala, Sweden
69. Physics Section, Division of Physical and Chemical Sciences, International Atomic Energy Agency, P.O. Box 100, Wagramer Strasse 5, A-1400 Vienna, Austria
70. Association EURATOM-Hellenic Republic, National Technical University of Athens, Iroon Politech niou 9, 157 73 Zografou, Athens, Greece
71. IPF, Stuttgart University, Stuttgart, Germany
72. University of Tartu, Ülikooli 18, 50090 Tartu, Estonia
73. University of Latvia, 19 Raina Blvd., Riga, LV 1586, Latvia
74. MIT Plasma Science and Fusion Centre, Cambridge, MA 02139, Massachusetts, USA
75. Association EURATOM-MHST, Jozef Stefan Institute, Reactor Physics Department, Jamova 39, SI-1000 Ljubljana, Slovenia
76. Moscow State University, Moscow 119991, Russian Federation
77. Association EURATOM-Risø National Laboratory, Technical University of Denmark, P.O.Box 49, DK-4000 Roskilde, Denmark
78. Departamento de Física, Universidad Carlos III de Madrid, 28911 Leganés, Madrid, Spain
79. Association EURATOM-VR, Department of Physics, SCI, KTH, SE-10691 Stockholm, Sweden
80. Statistical and Plasma Physics Unit, Association EURATOM-Belgian State, Université Libre de Bruxelles, Campus Plaine, CP 231, Boulevard du Triomphe, B-1050, Belgium
81. The “Horia Hulubei” National Institute for Physics and Nuclear Engineering, Association EURA TOM-MEdC, Magurele-Bucharest, Romania
82. Department of Physics and Applied Physics, University of Strathclyde, Glasgow, G4 ONG, UK
83. Associazione EURATOM-ENEA sulla Fusione, Politecnico di Torino, Italy
84. Department of Physics, University of Warwick, Coventry, CV4 7AL, UK
85. CEA/Saclay, F-91191 Gif-sur-Yvette CEDEX, France
86. Tampere University of Technology, Association EURATOM-Tekes, P.O. Box 527, FI-33101 Tampere, Finland
87. Association EURATOM-Belgian State Department of Data Analysis, Ghent University, 9000 Gent, Belgium
88. University of York, Heslington, York YO10 5DD, UK
89. Institute of Plasma Physics, Chinese Academy of Sciences, Hefei, 230031, China

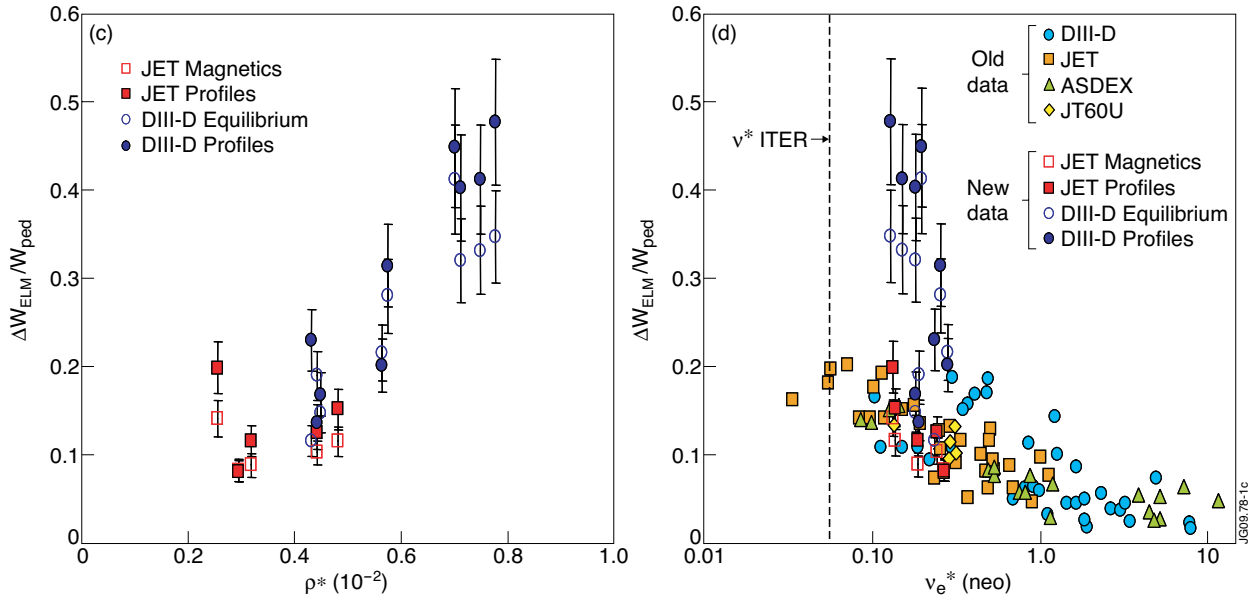

Figure 1: Fractional ELM losses from JET and DIII-D ρ scan as function of ρ* and ν*.*

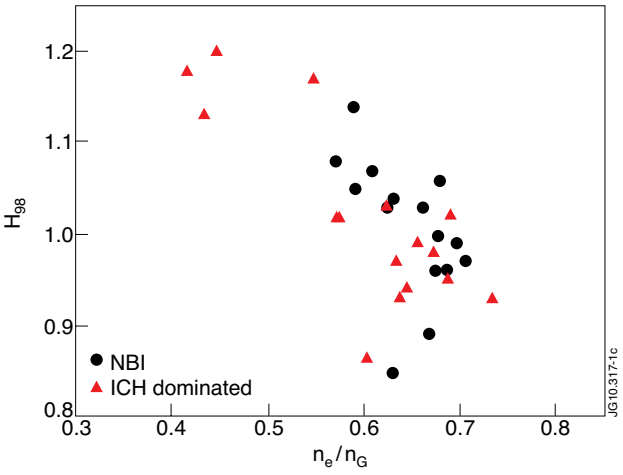

Figure 2: Confinement enhancement factor H98(y,2) versus normalised density.

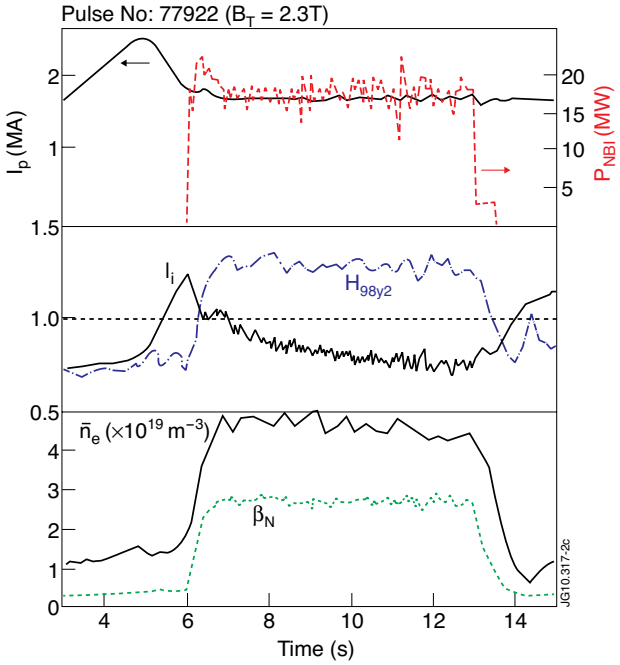

Figure 3: Hybrid discharge (δ~0.4) at 75% of the Greenwald density with H98y2 maintained at 1.3 for one resistive time.

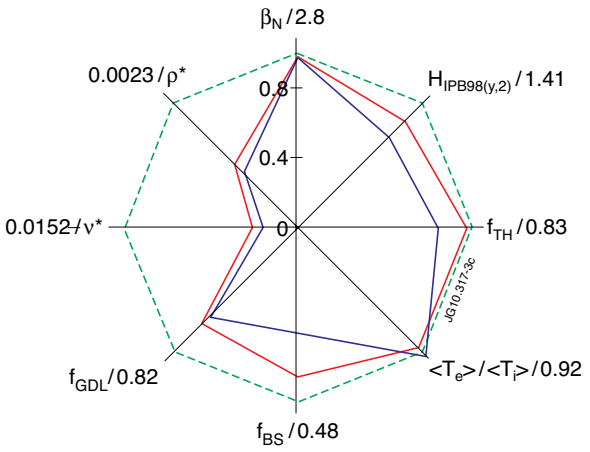

Figure 4: Dimensionless parameters for JET Pulse No: 78052, 1.8MA / 2.7 T (red) normalised to ITER SS targets compared to previously best performance, Pulse No: 70069 1.5MA/2.3T (blue).

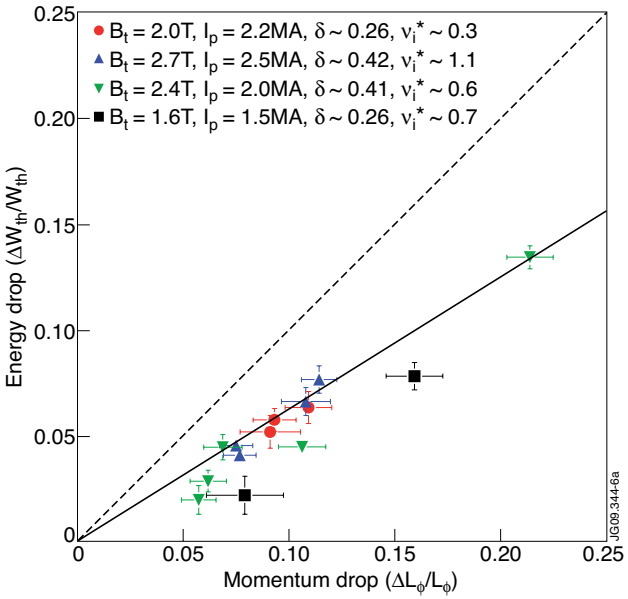

Figure 5: Normalised thermal energy drop versus normalised momentum drop per ELM.

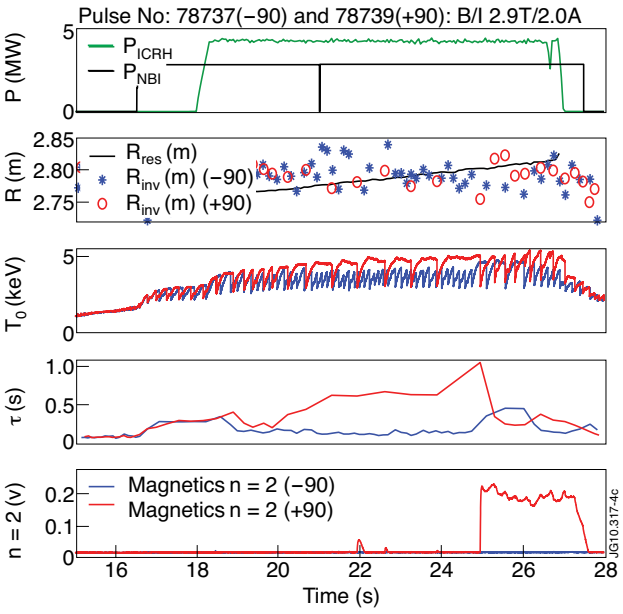

Figure 6: Sawtooth control with ^{3}He minority ICRH.

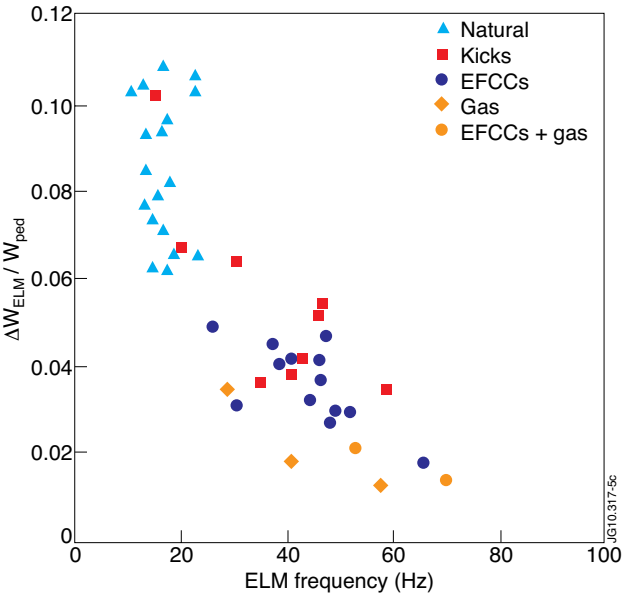

Figure 7: Normalized ELM energy loss (to the pedestal energy) versus ELM frequency (high δ, q_{95} = 3.6-3.9, P_{NBI} = 10-12MW).

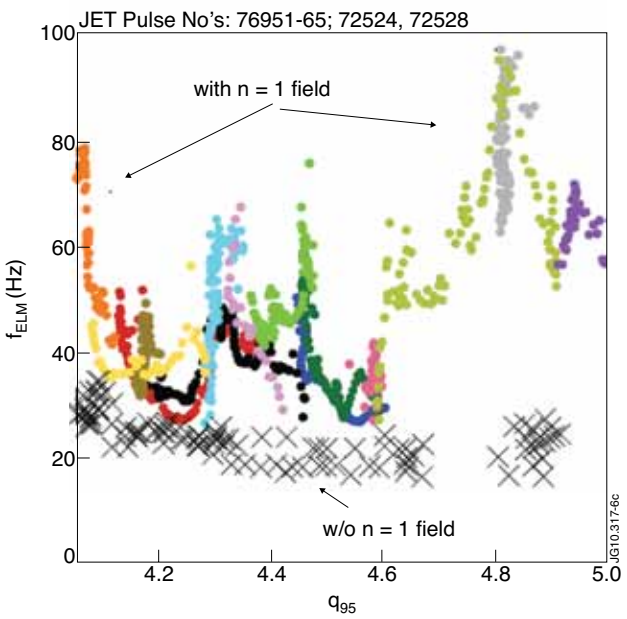

Figure 8: ELM frequency resonances in q_{95} with n=1 fields applied by EFCCs.

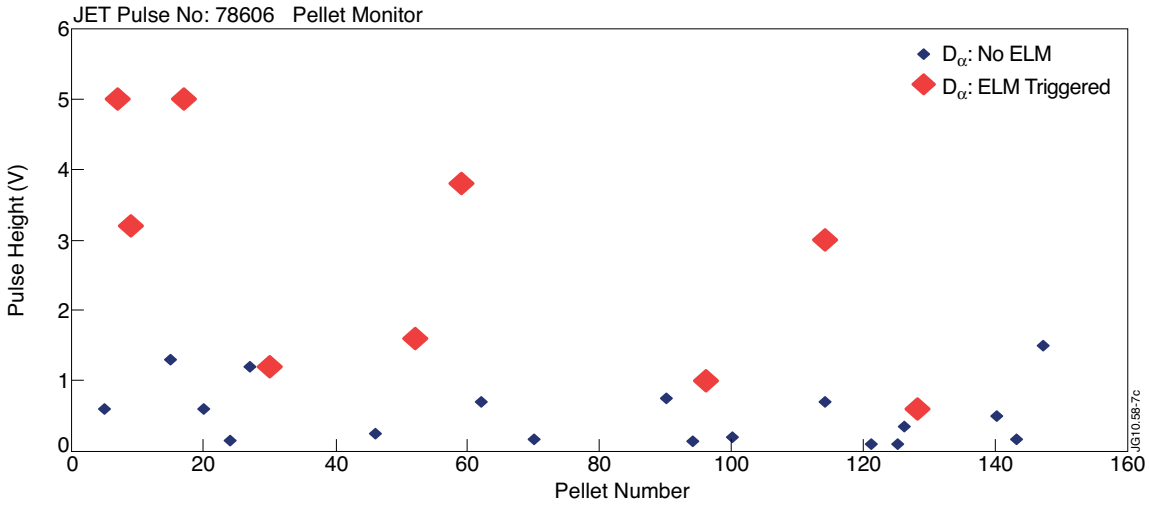

Figure 9: Pellet monitor (D_α) pulse height against pellet request. Pellets triggering an ELM shown in red. 1V pulse height corresponds to ~ 1 – 1.6×10^{19}D / pellet.

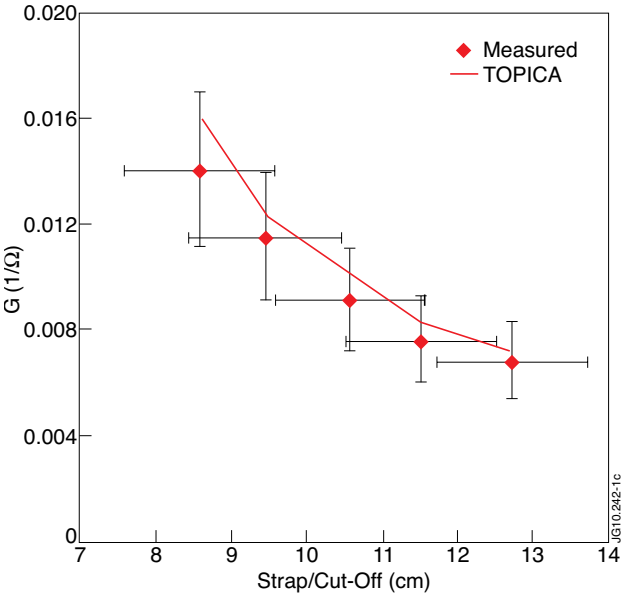

Figure 10: Root causes of JET disruptions.

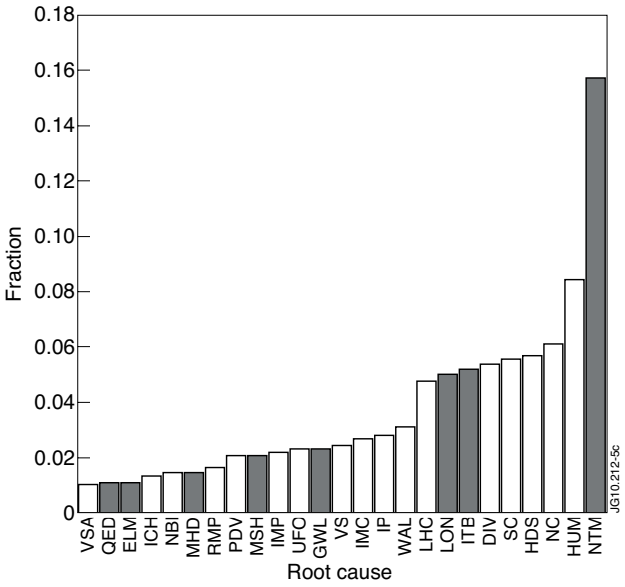

Figure 11: The coupling in terms of effective conductance calculated from TOPICA data. Representative error bars are shown of ±1cm on position and ±21% on power.